

## Article

# Zircon U-Pb Dating and Metamorphism of Granitoid Gneisses and Supracrustal Rocks in Eastern Hebei, North China Craton

Zhanzhan Duan <sup>1,2,\*</sup>, Chunjing Wei <sup>3</sup>, Zhuang Li <sup>4,5</sup> and Cong Zhang <sup>6</sup> 

<sup>1</sup> Hebei Key Laboratory of Strategic Critical Mineral Resources, Hebei GEO University, Shijiazhuang 050031, China

<sup>2</sup> College of Earth Sciences, Hebei GEO University, Shijiazhuang 050031, China

<sup>3</sup> MOE Key Laboratory of Orogenic Belts and Crustal Evolution, School of Earth and Space Sciences, Peking University, Beijing 100871, China; cjwei@pku.edu.cn

<sup>4</sup> State Key Laboratory of Petroleum Resources and Prospecting, China University of Petroleum (Beijing), Beijing 102249, China; lizhuangcc@pku.edu.cn

<sup>5</sup> College of Geosciences, China University of Petroleum (Beijing), Beijing 102249, China

<sup>6</sup> Key Laboratory of Deep-Earth Dynamics of MLR, Institute of Geology, Chinese Academy of Geological Sciences, Beijing 100037, China; congzhang@pku.edu.cn

\* Correspondence: duanzhan@pku.edu.cn

**Abstract:** Granitoid gneisses dominated by tonalitic–trondhjemitic–granodioritic (TTG) compositions, with metamorphic supracrustal rocks consisting of sedimentary and volcanic rocks, are widely exposed in the Eastern Hebei terrane, North China Craton (NCC). This study presents systematic zircon U–Pb geochronological and whole-rock geochemical data of the Neoproterozoic granitoid gneisses and supracrustal rocks in Eastern Hebei. Zircon U–Pb isotopic dating for the representative samples reveals that magmatic precursors of granitoid gneisses were emplaced between  $2524 \pm 7$  and  $2503 \pm 12$  Ma, and the protoliths of the pelitic granulites were deposited in the Late Neoproterozoic era. Both of them have been subjected to granulite facies metamorphism during  $2508 \pm 10$  to  $2468 \pm 33$  Ma, coeval with the intrusion of syenogranitic pegmatite ( $2488 \pm 5$  Ma). Zircon ages of 2.45–2.01 Ga obtained from the analyzed samples were considered mixed data from 2.53–2.48 Ga and 1.9–1.8 Ga and were chronologically meaningless. Paleoproterozoic metamorphic zircon ages of 1.9–1.8 Ga were usually neglected because of hardly being obtained from TTG gneisses and supracrustal rocks. The tectonic regime during the Neoproterozoic era was considered to be dominated by vertical tectonism in the Eastern Hebei terrane.

**Keywords:** granitoid gneiss; supracrustal rocks; zircon geochronology; tectonic setting; Eastern Hebei



**Citation:** Duan, Z.; Wei, C.; Li, Z.; Zhang, C. Zircon U-Pb Dating and Metamorphism of Granitoid Gneisses and Supracrustal Rocks in Eastern Hebei, North China Craton. *Minerals* **2022**, *12*, 863. <https://doi.org/10.3390/min12070863>

Academic Editor: Marion Tichomirowa

Received: 22 May 2022

Accepted: 4 July 2022

Published: 7 July 2022

**Publisher's Note:** MDPI stays neutral with regard to jurisdictional claims in published maps and institutional affiliations.



**Copyright:** © 2022 by the authors. Licensee MDPI, Basel, Switzerland. This article is an open access article distributed under the terms and conditions of the Creative Commons Attribution (CC BY) license (<https://creativecommons.org/licenses/by/4.0/>).

## 1. Introduction

Archean cratons are predominantly composed of granite-greenstone terranes [1]. Most of them display a dome-and-keel geometry, in which the supracrustal rocks occur as structural troughs wedged between dome-shaped bodies of the granitoid complex that are dominated by tonalitic, trondhjemitic and granodioritic gneisses [2]. It is still highly controversial whether the tectonic regime of Archean craton is dominated by horizontal or vertical tectonism [3–7]. Horizontal tectonism characterized by horizontal movements of rigid plates is considered to be connected to plate tectonics, which is accompanied by subduction, arc magmatism, paired metamorphic belts and continent-continent collision. Nevertheless, when plate tectonics emerged and how the style of the plate tectonics operated on earth is still up for debate [8–12]. Vertical tectonism is owing to density inversion characterized by buoyant rising of granitoids (diapirism) and sinking of denser volcanic sequences (sagduction) [13]. Some scholars thought that synchronous vertical and horizontal tectonism was a common process in the Neoproterozoic and might represent a transition from dominant vertical tectonism in the Paleoproterozoic-Mesoproterozoic to dominant horizontal

tectonism in the Proterozoic and Phanerozoic [14,15]. It is still controversial whether the vertical tectonism was still a dominant tectonic regime that was operating in the eastern North China Craton during the Late Neoproterozoic era [16].

The North China Craton (NCC), preserving ~3.85 Ga rocks, is one of the oldest cratonic blocks on earth [17–20], and was assembled through four micro-blocks with three Paleoproterozoic orogenic belts (Figure 1a) [21–24]. As a typical example of the Archean crust in the NCC, the Eastern Hebei terrane is composed predominantly of massive TTG gneisses, potassium-rich granitoids and minor dioritic gneisses, with supracrustal rocks consisting of ultramafic to felsic volcanic and sedimentary rocks [25–39]. The Eastern Hebei terrane had suffered multi-phase magmatic and tectono-thermal events and preserved a wide variety of Archean lithological associations. The Paleoproterozoic (~1.82 Ga) overprinting metamorphism of high-pressure granulite facies was predominantly identified from metabasic dykes [33,36]. However, the reason why Paleoproterozoic metamorphic ages were quite difficult to be obtained from the Archean rocks (e.g., TTG gneisses and pelitic granulites) has rarely been discussed before.

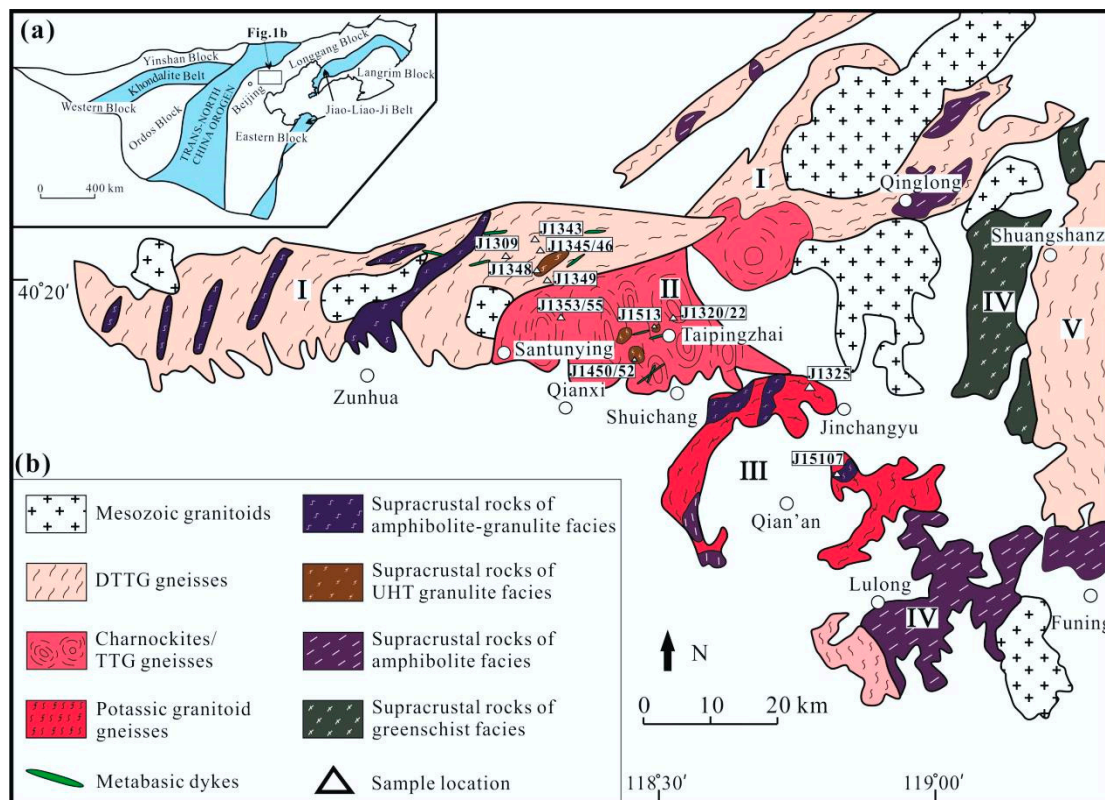


**Figure 1.** (a) Tectonic subdivision of the NCC [21] and the location of the study area. (b) Geological map of the Eastern Hebei terrane [40]. (I) the Saheqiao linear-structural belt; (II) The Taipingzhai ovate-structural domain; (III) The Qian'an gneiss dome; (IV) The Lulong–Shuangshanzi supracrustal belt; (V) The Anziling gneiss dome.

The Neoproterozoic tectonic setting and geodynamic evolution of the Eastern Hebei terrane remains controversial. Some researchers favor tectonic environment related to subduction-collision [41–44]. For example, according to Zhai and Santosh (2011) [41], the major period of continental growth during 2.9–2.7 Ga in the NCC correlates with the global growth of Earth's crust. The cratonization of the NCC through the amalgamation of micro-blocks along linear folded greenstone belts was completed by ca. 2.5 Ga, accompanied by granulite facies metamorphism [41]. Kusky et al. (2007, 2011) [42,43] proposed that Archean metamorphic basement of NCC can be divided into the Eastern Block, Central Orogenic Belt and Western Block. The Eastern and Western Blocks were formed by the collision of

microcontinents and arcs during 3.5–2.7 Ga. A long arc and accretionary prism collided with the margin of the Eastern Block at 2.5 Ga. Besides, Liu et al. (2018) [44] considered the Neoproterozoic basement rocks as typical subduction zone lithological assemblages and geochemical signature. The Late Archean tectonothermal events were regarded to have been generated under a typical Archean hot orogenic belt, evolving from subduction and back-arc extension to the final collision. Nutman et al. (2011) [28] identified three magmatic activity stages during Neoproterozoic, and proposed that the first two stages belonged to a typical island arc setting, whereas the last stage was consistent with crustal extension setting and was coupled with metamorphism of granulite facies. However, other researchers prefer a plume tectonic setting dominated the Neoproterozoic basement in eastern Hebei [22], which is supported by the following geological facts: (1) the extensive exposure of granitoid intrusions that formed during a short period (2.55–2.50 Ga), accompanied by granulite facies metamorphism; (2) dominant domal structures; (3) bimodal volcanic assemblages in the greenstone sequences; (4) metamorphism with anticlockwise P–T paths involving isobaric cooling; (5) affinities of mafic rocks to continental tholeiitic basalts. Alternatively, an Archean unique vertical tectonic model involving sagduction regime was proposed, supported by petrological observation, zircon chronology and metamorphic evolution of supracrustal rocks [34].

In this study, we present systematic petrological observations, new zircon U–Pb chronological data, and bulk-rock and zircon geochemical data for Neoproterozoic granitoid gneisses of dominant TTG compositions, supracrustal rocks involving mafic and pelitic granulites as well as pegmatite in Eastern Hebei. Integrating these data with previous studies, we discuss (i) two phase granulite facies metamorphism of the Neoproterozoic and Paleoproterozoic eras; (ii) zircon behaviors in high-grade rocks and (iii) tectonic setting and geodynamic evolution in the Eastern Hebei terrane during the Neoproterozoic era.

## 2. Geological Setting

The Eastern Hebei terrane can be divided into five litho-tectonic units (Figure 1b) [40]: (I) the Saheqiao linear-structural belt is composed predominantly of dioritic–tonalitic–trondhjemitic–granodioritic (DTTG) gneisses and minor supracrustal rocks. The DTTG gneisses show similar magmatic crystallization ages of 2.55–2.50 Ga and metamorphic ages of 2.47–2.31 Ga [25,45]. Recently, ~2.9 Ga magmatic event in Zunhua was identified by the results of a comprehensive isotopic investigation of zircons from metamorphosed felsic gneisses and amphibolites [46]. The supracrustal rock series comprise mainly mafic granulites and amphibolites with a few ultramafic, pelitic and Banded Iron Formations (BIF) interlayers [47]. Zircon dating of mafic granulites, amphibolites and BIFs yielded magmatic crystallization ages of 2.61–2.52 Ga and metamorphic ages of 2.53–2.47 Ga and 1.97–1.83 Ga [29,36]. The older metamorphic ages are thought to represent two-pyroxene granulite facies metamorphism in Neoproterozoic era, while the Paleoproterozoic metamorphic ages indicate an overprinting metamorphism of high-pressure granulite facies [36]. (II) The Taipingzhai ovate-structural domain is characterized by a series of ovate structure and composed of Neoproterozoic (2.58–2.50 Ga) TTG gneisses, charnockites with minor mafic granulites, sillimanite-garnet plagioclase gneiss and BIFs [45]. The supracrustal rocks were interlayered with BIF and occurred as small enclaves or rafts in TTG gneisses. The mafic granulites has peak P–T conditions of 9.6–10.3 kbar/860–900 °C with anticlockwise P–T path [31]. The sillimanite-garnet plagioclase gneiss has peak P–T conditions of 12–13 kbar/820–850 °C with clockwise P–T path [39]. However, recent studies suggest that both mafic and pelitic granulites in Taipingzhai area reached to ultra-high temperature (UHT) metamorphism at their peak stage with P–T conditions of 9 kbar/1025–1060 °C [34]. (III) The Qian'an gneiss dome comprises TTG gneisses, charnockites and potassic granitoid gneisses [28]. The emplacement ages of TTG and granitic gneisses were 2.55–2.49 Ga, but a few at 3.28–2.94 Ga [27,48]. (IV) The Lulong–Shuangshanzi supracrustal belt was composed of Neoproterozoic (2.56–2.50 Ga) paragneiss and gneissic migmatite of amphibolite facies [49,50]. (V) The Anziling gneiss dome comprises mainly of TTG gneiss and

several supracrustal enclaves. The TTG gneisses were emplaced at 2.53–2.50 Ga and metamorphosed at 2.50–2.49 Ga [26] under amphibolite–granulite facies [28]. Some mafic dykes in the Saheqiao linear-structural belt and the Taipingzhai ovate-structural domain, cross-cutting the foliation of Archean DTTG gneisses and supracrustal rocks and yielding magmatic emplacement age of  $\sim$ 2.10 Ga and metamorphic age of  $\sim$ 1.82 Ga, went through HP granulite facies metamorphism with clockwise P-T path [33,36].

### 3. Petrography and Analytical Methods

#### 3.1. Sampling Strategy

Fifteen rock samples were collected from Saheqiao, Taipingzhai and Jinchangyu regions. The samples comprise syenogranite (J1309), orthogneisses (J1320/22/25/43/45/46/49/53/55), mafic granulites (J1348) and pelitic granulites (J1513/15107, J1450/52). They were chosen for detailed petrographic and bulk-rock geochemical analyses. Representative samples (J1309/20/49/53 and J1513/15107) were chosen for zircon U–Th–Pb geochronological and trace element analyses. Field photographs and photomicrographs showing geological relationships and lithological features for the representative samples are present in Figures 2 and 3.



**Figure 2.** Field photographs of the representative rocks from Eastern Hebei. (a) metasupracrustal rocks intruded by syenogranitic pegmatite; (b) tonalitic gneiss, showing inhomogeneous petrological feature with melanocratic and leucocratic domains distributed randomly; (c) dioritic gneiss; (d) granodioritic gneiss; (e) mafic granulite and leucosome generated during granulite facies metamorphism; (f) pelitic granulite with felsic vein formed by partial melting.

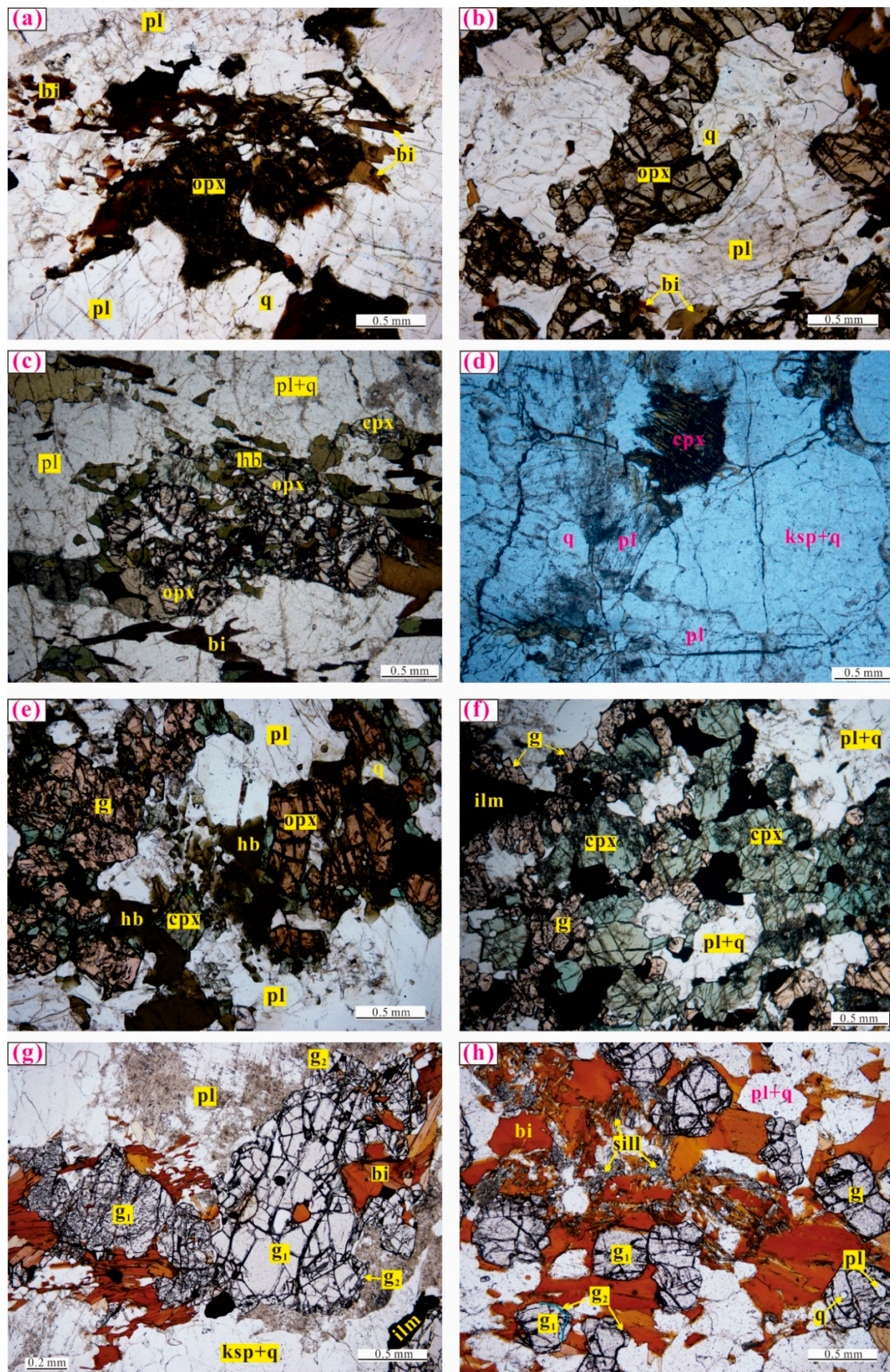


**Figure 3.** Photomicrographs showing petrographic features of representative samples (under plane polarized light). (a) J1353A (felsic minerals domain), granodioritic gneiss; (b) J1353B (mafic mineral

domain), dioritic gneiss; (c) J1349, monzodioritic gneiss; (d) J1320, tonalitic gneiss; (e) J1348A, mafic granulite; (f) J1348B, mafic granulite; the fine-grained garnet showing typical of 'red-eye socket' texture around pyroxene and plagioclase; (g) J1513 felsic paragneiss; the overprinting assemblage characterized by  $g_2$  (surrounded by coarse-grained garnet porphyroblast); (h) sillimanite-bearing pelitic granulite consisting of garnet, sillimanite, biotite, plagioclase, K-feldspar and quartz; the overprinting assemblage characterized by  $g_2$  being visible. Mineral abbreviations are as follows: pl, plagioclase; hb, hornblende; q, quartz; ksp, K-feldspar; g, garnet; bi, biotite; opx, orthopyroxene; cpx, clinopyroxene; sill, sillimanite and ilm, ilmenite.

### 3.2. Petrography

Syenogranitic pegmatite, consisting of coarse-grained orthoclase, quartz and minor plagioclase, intruded into the metasedimentary rocks (Figure 2a). The orthogneisses are mainly composed of TTG gneisses, dioritic and a few monzonitic gneisses. The tonalitic-dioritic gneisses are characterized by inhomogeneous petrological appearance with melanocratic pyroxene-amphibole-biotite domains and leucocratic feldspar-quartz domains distributed randomly (Figure 2b,c). The granodioritic and trondhjemitic gneisses are relatively homogeneous (Figure 2d) and are composed mainly of plagioclase, quartz and a few pyroxene grains. The leucosomes, generated by partial melting, are present commonly both in mafic and pelitic granulites (Figure 2e,f).

Tonalitic-dioritic gneisses show the mineral assemblage of clinopyroxene, plagioclase, orthopyroxene, amphibole, biotite, quartz and ilmenite. The oriented arrangement of biotite and/or amphibole gives rise to the foliation of gneisses. The peak assemblages of  $opx + pl \pm cpx$  indicate that they have undergone granulite facies metamorphism (Figure 3a,b), followed by retrograde metamorphism of amphibolite facies evidenced by amphibole crossing the clinopyroxene and orthopyroxene (Figure 3c,d). Two generations of mineral assemblage are distinguished in mafic granulite. The first generation includes medium-grained  $cpx + opx + pl$ , while the second generation is characterized by the fine-grained garnet showing typical of 'red-eye socket' texture around pyroxene and plagioclase (Figure 3e,f). These two generations of mineral assemblage were considered to represent two phases of granulite facies metamorphism in Neoproterozoic and Paleoproterozoic, respectively [33]. The pelitic granulite assemblages include garnet, k-feldspar, biotite, plagioclase, quartz, sillimanite and orthopyroxene (Figure 3g,h). The assemblages on the retrograde fluid-absent solidus in granulites with presence of biotite are nominated as final assemblages [36], which can be differentiated from the peak assemblages through detailed petrographic observations. Thus, four generations of assemblages are identified from pelitic granulites, involving final, peak, inclusion and overprinting stages. The final assemblage is characterized by presence of matrix biotite, while the peak assemblage is characteristic of the absence of the matrix biotite. The inclusion assemblage is characterized by plagioclase and biotite inclusions in garnet. The overprinting assemblage, characteristic of fragmentary coronary garnet ( $g_2$ ) around porphyroblastic garnet ( $g_1$ ), was considered to be formed coeval with the 'red-eye socket' garnet, which represents the products of the Paleoproterozoic overprinting metamorphism.

### 3.3. Analytical Methods

Seventeen representative samples were washed and chipped to remove any weathered surfaces, and the fresh surfaces were pulverized to 200-mesh size in an agate mill. The bulk-rock compositions were determined by ICP-OES analysis at China University of Geoscience (Beijing) and relative standard deviations of the analytical data are better than 5%. The results are presented in Table 1.

**Table 1.** Whole-rock geochemical compositions of representative samples from Eastern Hebei.

Sample Number	ICP-OES Whole Rock Compositions (wt.%)												
	SiO <sub>2</sub>	TiO <sub>2</sub>	Al <sub>2</sub> O <sub>3</sub>	FeO <sub>T</sub>	MnO	MgO	CaO	Na <sub>2</sub> O	K <sub>2</sub> O	P <sub>2</sub> O <sub>5</sub>	LOI	A/CNK	Mg#
J1309	74.83	0.02	13.81	0.22	0.00	0.03	0.59	2.88	6.59	0.04	0.38	1.07	0.21
J1320	71.45	0.04	16.62	0.73	0.01	0.35	3.75	4.57	1.06	0.11	0.55	1.07	0.49
J1343	70.47	0.49	16.89	1.44	0.01	0.34	1.27	5.23	2.03	0.11	1.14	1.29	0.32
J1346	60.43	0.54	17.04	6.35	0.09	3.31	5.87	4.34	0.66	0.07	0.96	0.92	0.51
J1325	68.47	0.31	14.94	2.71	0.03	1.11	1.93	3.72	4.61	0.11	1.47	1.02	0.45
J1345	63.81	0.43	17.08	4.55	0.07	1.98	4.18	4.32	1.07	0.10	1.66	1.08	0.47
J1322	59.98	0.44	15.95	6.26	0.09	3.36	6.08	3.98	1.13	0.25	1.61	0.85	0.52
J1353A	67.42	0.33	14.72	3.95	0.04	2.11	2.45	3.03	4.59	0.11	0.58	1.02	0.52
J1353B	57.43	0.75	15.49	9.90	0.09	5.29	3.66	3.63	2.74	0.24	0.18	0.99	0.52
J1355	59.36	0.20	7.71	24.69	0.08	1.69	1.78	1.05	2.18	0.19	0.30	1.05	0.12
J1349	50.91	0.72	17.88	9.11	0.12	5.03	7.37	4.36	1.79	0.37	1.60	0.79	0.52
J1348A	56.36	0.71	16.32	9.18	0.10	3.93	6.92	3.99	0.85	0.13	0.74	0.81	0.46
J1348B	49.53	1.65	12.87	16.71	0.28	5.05	9.86	2.45	0.55	0.15	0.66	0.57	0.38
J1513	66.29	0.72	15.53	4.80	0.04	2.08	2.69	3.71	2.62	0.08	0.75	1.12	0.46
J15107	63.15	0.74	15.42	10.71	0.08	3.76	1.99	1.86	1.94	0.12	0.50	1.75	0.41
J1450	62.08	0.65	16.10	8.85	0.11	3.86	3.47	2.94	0.89	0.13	0.32	1.33	0.47
J1452	64.12	0.89	16.36	5.94	0.08	3.07	2.89	3.81	1.67	0.09	0.79	1.23	0.51

A/CNK (molar Al<sub>2</sub>O<sub>3</sub>/(CaO + Na<sub>2</sub>O + K<sub>2</sub>O)); Mg# (molar MgO/(MgO + FeO<sub>total</sub>)).

Zircon U–Pb isotopes and REE geochemistry were simultaneously analyzed by the laser ablation–inductively coupled plasma–mass spectrometry (LA–ICP–MS) method. Zircon grains were separated by conventional heavy-liquid and magnetic separation methods, followed by hand-picking under a binocular microscope. Zircon grains were set in an epoxy mount, polished, and then vacuum-coated with a layer of 50 nm high-purity gold. Cathodoluminescence (CL) images were obtained for zircons using a FEI PHILIPS XL 30 SEFG SEM with 2-min scanning time under conditions of 15 kV and 120 μA at the SEM Laboratory of the Peking University, in order to characterize internal structures and choose potential target sites. The zircon LA–ICP–MS U–Pb isotopic analyses were performed at the Key Laboratory of Orogenic Belts and Crustal Evolution, Peking University. Zircon 91,500 was used as an external standard for all U–Th–Pb isotopic analyses, and the standard has the average apparent <sup>207</sup>Pb/<sup>206</sup>Pb age of 1063 ± 35 Ma [51]. The Plešovice zircon was used as a secondary standard with the average apparent <sup>206</sup>Pb/<sup>238</sup>U age of 337 ± 0.9 Ma. The concentrations of U, Th and Pb elements were calibrated using <sup>29</sup>Si as an internal calibrant and NIST 610 as an external reference standard. The correction for common lead content followed the LA–ICP–MS Common Lead Correction (ver. 3.15) method of Andersen (2002) [52]. <sup>207</sup>Pb/<sup>206</sup>Pb, <sup>206</sup>Pb/<sup>238</sup>U and <sup>207</sup>Pb/<sup>235</sup>U ratios and apparent ages were calculated using the GLITTER 4.4 [53]. The age calculations and Concordia plots were made using Isoplot [54]. The size of a single spot of ablation was approximately 32 μm. Uncertainties on individual LA–ICP–MS analyses are quoted at the 1 sigma level, with errors on pooled ages at the 95% confidence level. Zircon U–Pb isotopic data, analyzed ages and REE data are listed in Supplementary Tables S1 and S2.

## 4. Results

### 4.1. Whole-Rock Chemical Compositions

The geochemical data listed in Table 1 are analyzed from various rock samples, including syenogranitic pegmatite, orthogneisses with variable chemical compositions from mafic to acidic, two mafic granulites and four pelitic granulites. Samples J1353 and 1348 show patchy appearance, and the felsic veins (J1353A and J1348A) and mafic mineral enriched

domains (J1353B and J1348B) are separated to be analyzed, respectively. The syenogranitic pegmatite sample possesses  $\text{SiO}_2$ ,  $\text{Al}_2\text{O}_3$ ,  $\text{K}_2\text{O}$ ,  $\text{Na}_2\text{O}$ , and  $\text{CaO}$  contents of 74.83%, 13.81%, 6.59%, 2.88%, and 0.59%, with a wide range of A/CNK (molar  $\text{Al}_2\text{O}_3/(\text{CaO} + \text{Na}_2\text{O} + \text{K}_2\text{O})$ ) ratio of 1.07. In the total alkali versus silica (TAS) diagram, it plots in the granite field (Figure 4a). Orthogneiss samples show variable  $\text{SiO}_2$  contents of 50.91%–71.45%, with a wide range of A/CNK ratios (0.79–1.29) and Mg# (molar  $\text{MgO}/(\text{MgO} + \text{FeO}_{\text{total}})$ ) ratios from 0.12–0.52. Most of them plot in the diorite, granodiorite and granite fields, except sample J1349 and J1353B in the monzodiorite and monzonite fields, respectively. Sample J1348B have lower  $\text{SiO}_2$ , higher  $\text{FeO}_{\text{total}}$ ,  $\text{MgO}$  and  $\text{CaO}$  contents of 49.53%, 16.71%, 5.05% and 9.86% compared with sample J1348A, and they plot in the gabbro and gabbro-diorite fields. Four pelitic granulites have similar geochemical compositions and plot in the granodiorite field. According to the An–Ab–Or diagram, granitoid gneisses plot on the trondhjemite, tonalite and granodiorite fields, indicating they have chemical components of the TTG magmatic suite (Figure 4b).

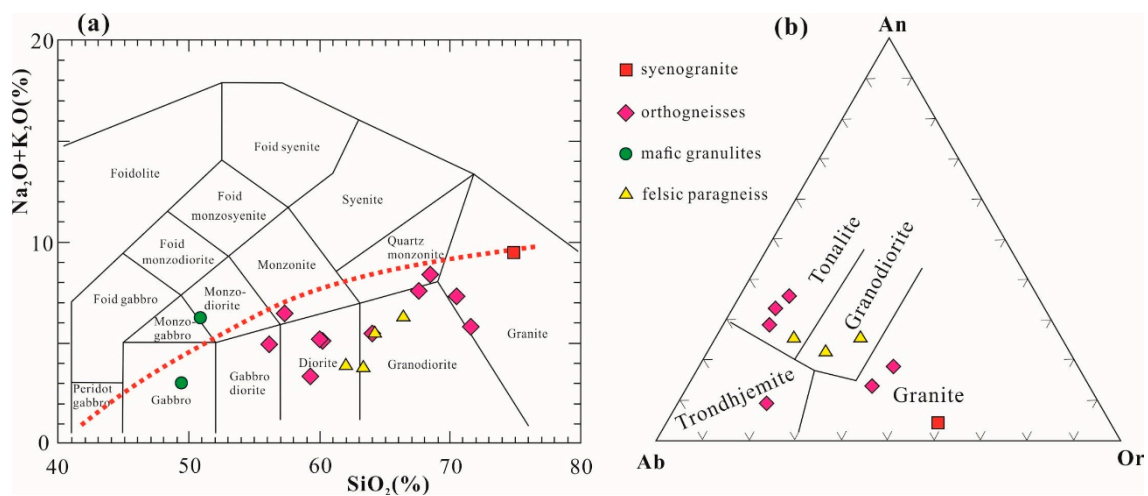


**Figure 4.** Geochemical classification diagrams for the analyzed representative samples in Eastern Hebei. (a) Total alkali versus silica (TAS) diagram [55]; (b) An–Ab–Or diagram [56].

## 4.2. Zircon U–Pb Isotopes

### 4.2.1. Sample J1309 (Syenogranitic Pegmatite)

Zircons from sample J1309 have grain sizes of 60–280  $\mu\text{m}$  with long prismatic or irregular shapes. In CL images, most grains exhibit blurry banded structure and a few display oscillatory zoning with dark luminescence suggesting their high U contents (Figure 5a). Thirty-three U–Pb isotopic analyses were conducted on 33 zircon grains. The obtained analyses are plotted on or below the concordia curve (Figure 6a), yielding a weighted mean  $^{207}\text{Pb}/^{206}\text{Pb}$  ages of  $2488 \pm 5$  Ma (MSWD = 0.93) with Th/U ratios of 0.25–0.76. Therefore, we considered 2488 Ma as the crystallization age of the syenogranitic pegmatite.

### 4.2.2. Sample J1320 (Tonalitic Gneiss)

Zircon grains from tonalitic gneiss exhibit long prismatic shapes with length and length/width ratios of 80–210  $\mu\text{m}$  and 3:2–2:1, respectively. Most of them show core-rim structure, which cores have an oscillatory zoning structure surrounded by homogeneous bright rims (e.g., spot #4, #5; Figure 5b). Forty-one U–Pb analyses were undertaken on 35 grains. Thirty analyses undertaken on the oscillatory zoned zircon show apparent  $^{207}\text{Pb}/^{206}\text{Pb}$  ages from 2416 to 2607 Ma. Three analyses with the oldest  $^{207}\text{Pb}/^{206}\text{Pb}$  dates of 2587 to 2607 Ma were thought to be conducted on zircon grains that were captured from the surrounding ancient rocks. Nineteen analyses yielded a weighted mean  $^{207}\text{Pb}/^{206}\text{Pb}$  ages of  $2510 \pm 13$  Ma (MSWD = 3.2) (Figure 6b). This is interpreted as the age of the tonalite protolith. The remaining eight analyses showed a wide dispersion in  $^{207}\text{Pb}/^{206}\text{Pb}$  dates beyond analytical error, from 2416 to 2492 Ma. This is interpreted as due to ancient

radiogenic Pb-loss. Eleven analyses of outer dull and bright rims yielded a weighted mean  $^{207}\text{Pb}/^{206}\text{Pb}$  ages of  $2508 \pm 10$  Ma (MSWD = 0.99) with Th/U ratios of 0.07–1.24, which is interpreted as the timing of granulite facies metamorphism.

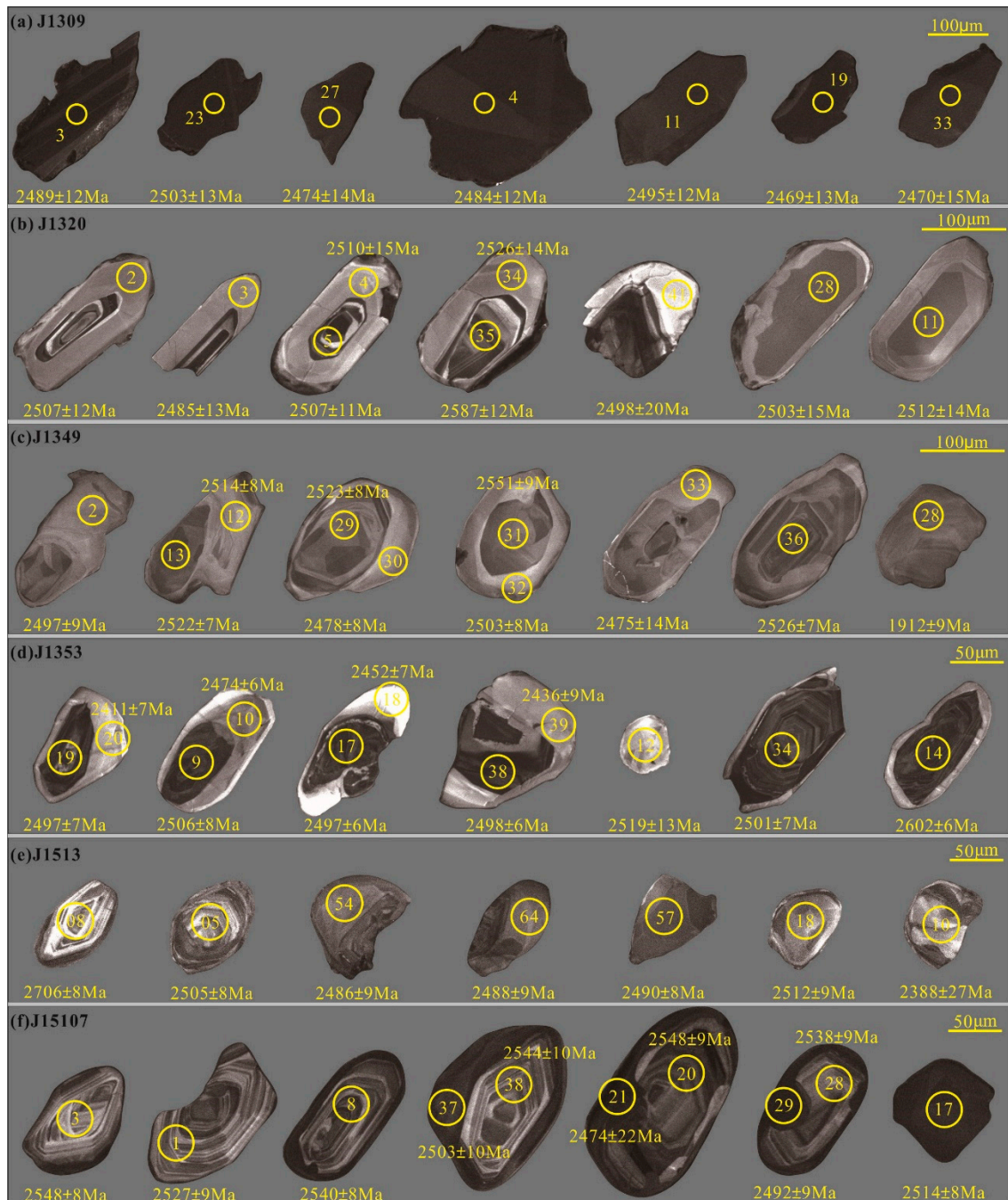


**Figure 5.** CL images of representative zircon grains showing analyzed locations, internal structures and apparent  $^{207}\text{Pb}/^{206}\text{Pb}$  ages. The solid circles in CL images show positions of LA-ICP-MS analytical sites, with their identification numbers as in Table S1, Th/U ratios and ages in Ma, respectively. (a) J1309 syenogranite; (b–d) J1320, J1349, J1353 orthogneisses; (e,f) J1513, J15107 felsic paragneisses.

#### 4.2.3. Sample J1349 (Dioritic Gneiss)

A total of forty analyses were performed on 34 zircon grains that showed prismatic, oval or irregular shape, and are 70–180 µm across with length/width ratios of 1:1–3:2. In CL images, they show core-rim structure with blurry oscillatory zoning, banded or

structureless dark domains in the cores, but relatively bright metamorphic rims (spot #29, #30; Figure 5c). Eighteen analyses undertaken on oscillatory zoning domains, with Th/U ratios of 0.50–0.97, form a linear array ranging from concordant to discordant (Figure 6c), indicative of different degrees of radiogenic Pb-loss. Fifteen analyses with older  $^{207}\text{Pb}/^{206}\text{Pb}$  dates yielded a weighted mean  $^{207}\text{Pb}/^{206}\text{Pb}$  ages of  $2524 \pm 7$  Ma (MSWD = 2.8). This is considered as the emplacement age for the magmatic precursor of monzodioritic gneiss. The remaining 22 analyses performed on metamorphic rim gave a wide range of apparent  $^{207}\text{Pb}/^{206}\text{Pb}$  dates from 2275 to 2542 Ma. After rejecting nine analyses which might have suffered strong ancient loss of radiogenic Pb, the remaining 12 analyses yielded a weighted mean  $^{207}\text{Pb}/^{206}\text{Pb}$  ages of  $2501 \pm 9$  Ma (MSWD = 1.9) with Th/U ratios being 0.41–0.81, which is considered as the timing of regional granulite facies metamorphism. Analysis (spot #28) gave the youngest and concordant  $^{207}\text{Pb}/^{206}\text{Pb}$  ages of  $1912 \pm 9$  Ma, further proving that Paleoproterozoic metamorphic event did occur in Eastern Hebei [32].

#### 4.2.4. Sample J1353 (Granodioritic Gneiss)

Zircon grains extracted from sample J1353 range in length from 40 to 130  $\mu\text{m}$ , with length to width ratios between 1:1 and 3:1. The majority of grains are prismatic, irregular and spherical in shape. The CL images reveal that zircon grains exhibit inner structures with oscillatory zoning (e.g., spot #34, #14, Figure 5d) or black inner cores, and invariably containing relatively bright metamorphic rims of variable width (<5 to 35  $\mu\text{m}$ ). A few grains have blurry fir-leaf zoning (spot #12). A total of 40 analyses were performed on 34 zircon grains. Twenty-six analyses performed on zircon cores with oscillatory zoning define three age groups on a  $^{206}\text{Pb}/^{238}\text{U}$ – $^{207}\text{Pb}/^{235}\text{U}$  concordia diagram (Figure 6d). The oldest group (2.60–2.55 Ga) is considered as the timing of xenocryst zircon grain that was captured from the ancient wall rocks around the channel during the magma's ascent. The second group consisting of 14 analyses are plotted on or below the concordia curve, yielding a weighted mean  $^{207}\text{Pb}/^{206}\text{Pb}$  age of  $2503 \pm 12$  Ma (MSWD = 3.7). We suggest that this age of 2504 Ma represents the magmatic crystallization age of the granodioritic gneiss sample. The remaining 8 analyses gave younger  $^{207}\text{Pb}/^{206}\text{Pb}$  age from 2331 to 2445 Ma, which is considered to be a result of heterogeneous Pb loss and has no geological significance. Fourteen analyses conducted on metamorphic rims yielded a weighted mean  $^{207}\text{Pb}/^{206}\text{Pb}$  age of  $2468 \pm 33$  Ma (MSWD = 25) after rejecting 5 analysis which might have suffered ancient loss of radiogenic Pb. This is interpreted as the time of granulite facies metamorphism.

#### 4.2.5. Sample J1513 (Pelitic Granulite)

A total of eighty spots were analyzed on 75 zircon grains whose lengths ranged from 40 to 110  $\mu\text{m}$  with length/width ratios of 1:1 to 3:1 (Figure 5e). The CL images show that these irregular or oval zircons have (i) clear oscillatory zoning (e.g., spots #5, #8), (ii) core-rim structure, where the inner cores show blurred oscillatory zoning with metamorphic growth rims (spot #54, 64), and (iii) sector or irregular zoning (spot #18, #57). Due to their abnormal signals, four spots (#1, #20, #69, #72) were removed for age calculation. The remaining 76 analyses give a wide range of apparent  $^{207}\text{Pb}/^{206}\text{Pb}$  dates from 2259 to 2706 Ma. We divided them into three age groups. The first group comprises 39 analyses of oscillatory-zoning inner cores whose apparent  $^{207}\text{Pb}/^{206}\text{Pb}$  dates range from 2462 to 2706 Ma. They are plotted on or under the concordia curve. The second group consists of thirteen analyses of sector zoning and metamorphic rims, with apparent  $^{207}\text{Pb}/^{206}\text{Pb}$  dates of 2447 to 2516 Ma and Th/U ratios of 0.02–0.33. These analyses are plotted on the concordia diagram and yielded a weighted mean  $^{207}\text{Pb}/^{206}\text{Pb}$  age of  $2485 \pm 10$  Ma (MSWD = 3.2) (Figure 6e), coeval with the regional granulite facies metamorphism. The third group is composed of eighteen spots with younger and discordant  $^{207}\text{Pb}/^{206}\text{Pb}$  dates of 2088 to 2443 Ma, which is interpreted as a result of heterogeneous Pb loss and has no geological significance.

#### 4.2.6. Sample J15107 (Sillimanite-Bearing Pelitic Granulite)

Forty U-Th-Pb isotopic analyses were carried out on 32 zircon grains from this sample. Zircon grains exhibit short prismatic and oval or irregular shapes with lengths of 60–150  $\mu\text{m}$  and length/width ratios of 1:1 to 3:1. In CL images, most zircon grains have oscillatory zoning with inner cores (e.g., spot #1, #3, #8, #38, Figure 5f) surrounded by low luminescence rims of varying thickness (spot #20, #37, #28), suggesting a magmatic origin of inner cores and then growth under metamorphic/thermal events [57,58]. A few grains show homogeneous with dark luminescence (e.g., spot #17), probably suggesting their metamorphic origin. All analyses have Th/U ratios of 0.01–1.17 and apparent  $^{207}\text{Pb}/^{206}\text{Pb}$  dates ranging from 2410 to 2584 Ma, and they display three age groups on the probability density diagram. The first group contains 31 analyses of oscillatory-zoned cores, yielding apparent  $^{207}\text{Pb}/^{206}\text{Pb}$  dates of 2410 to 2584 Ma with Th/U ratios of 0.19–1.17, and plots on or below the concordia curve. The second group is composed of 7 analyses of metamorphic overgrowth rim and homogeneous grain with low luminescence, yielding apparent  $^{207}\text{Pb}/^{206}\text{Pb}$  dates of 2474 to 2506 Ma and low Th/U ratios of 0.01–0.10. On a  $^{207}\text{Pb}/^{235}\text{U}$ - $^{206}\text{Pb}/^{238}\text{U}$  concordia diagram, they plot on or below the concordia curve, yielding a weighted mean age of  $2494 \pm 7$  Ma (MSWD = 1.09) (Figure 6f). Therefore, 2494 Ma is considered as the metamorphic age of the sill-bearing pelitic granulite sample. The remaining two analyses gave the youngest  $^{207}\text{Pb}/^{206}\text{Pb}$  ages of 2431 Ma and 2410 Ma with strong Pb loss.

#### 4.3. Zircon REE Compositions

Zircon grains of magmatic origin from syenogranitic pegmatite have significantly high chondrite-normalized REE values and the heavy rare earth element (HREE) contents are particularly high, leading to left-facing steep slopes on the chondrite-normalized REE plots (Figure 7a). These negative Eu anomaly in the REE pattern imply the major role of feldspar fractionation prior to (or during) zircon crystallization. Zircon grains from the orthogneisses (J1320, J1349 and J1353) have slightly lower chondrite-normalized REE values and HREE contents compared to those in syenogranitic pegmatite (Figure 7b–d). Zircons from the orthogneisses show enrichment in HREE and depleted in light-REE (LREE), exhibiting left-facing slopes on the chondrite-normalized REE plots. The HREE contents of metamorphic zircon grains are invariably lower than those in magmatic zircon, and this diagnostic feature is expected to be very robust to evaluate the genesis of zircon grains in high grade metamorphic rocks [30]. The majority of zircon grains no matter magmatic or metamorphic origin, exhibit negative Eu anomaly in their REE patterns, suggesting simultaneous or subsequent crystallization relative to feldspars. A few grains from samples J1320 and J1353 show positive Eu anomaly, which might be generated in residual melts if titanite also fractionates. Detrital zircons of magmatic origin have similar REE features to those from orthogneisses, but exhibiting variable chondrite-normalized REE values (Figure 7e,f). Metamorphic zircons from pelitic granulites have low chondrite-normalized REE values, characterised by a flat HREE pattern which indicates that these zircon grains are in equilibrium with garnet being generated during granulite facies metamorphism [59].

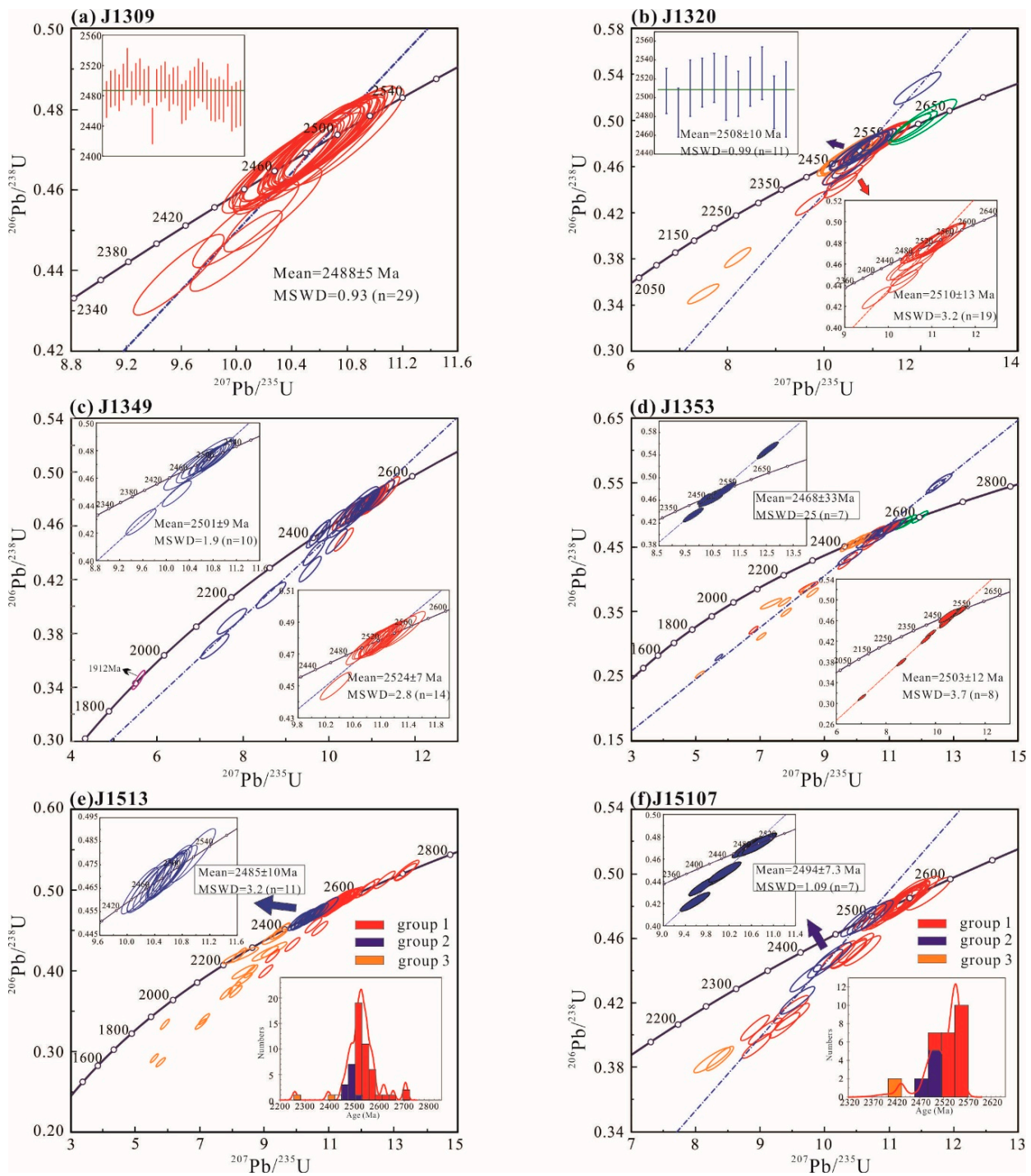


**Figure 6.** Concordia diagrams and histograms of apparent  $^{207}\text{Pb}/^{206}\text{Pb}$  ages of LA-ICP-MS U-Pb data for zircons from representative samples, Eastern Hebei. (a) J1309 syenogranite; (b–d) J1320, J1349, J1353 orthogneisses; (e,f) J1513, J15107 felsic paragneisses.

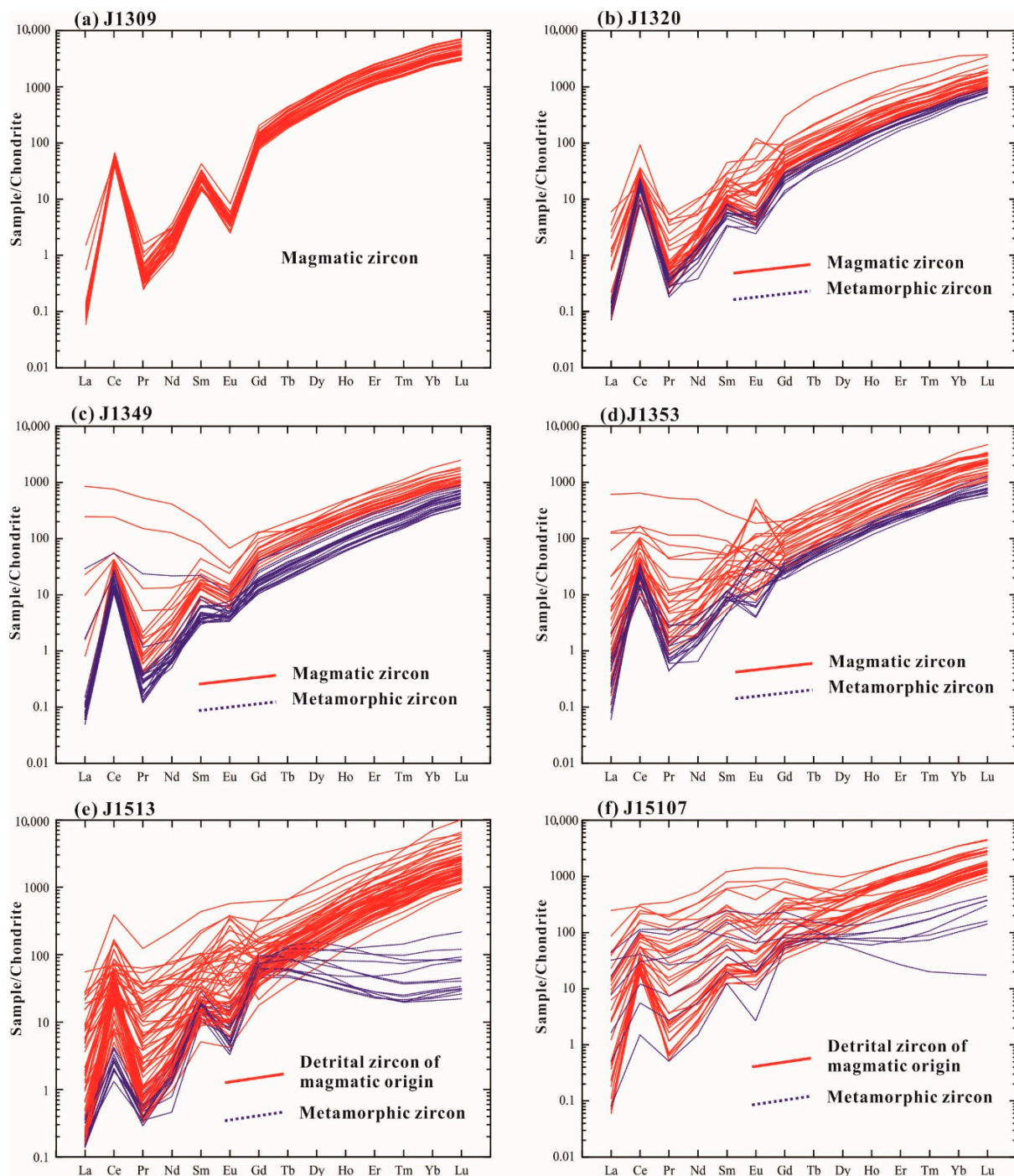


**Figure 7.** Chondrite-normalized REE patterns [44] for zircons of magmatic (solid red lines) and metamorphic origin (dashed blue lines) for analyzed samples from Eastern Hebei. The values of chondrite are from [60]. (a) J1309 syenogranite; (b–d) J1320, J1349, J1353 orthogneisses; (e,f) J1513, J15107 felsic paragneisses.

## 5. Discussion

### 5.1. Zircon U–Pb Ages and Two Phases of Granulite Facies Metamorphism

#### 5.1.1. Zircon U–Pb Ages

The metamorphic basement rocks in Eastern Hebei went through long geological evolution accompanied by polyphase magmatic and tectono-thermal events. Thus, the zircon U–Pb ages obtained from samples show a wide age span from 3.88 to 1.78 Ga [25–30,32–37].

The older ages are common especially in the supracrustal rocks, like fuchsite-bearing quartzite, in the Caozhuang and Huangbaiyu region. Most granitoid gneisses analyzed in this study contain abundant 2.55–2.45 Ga zircons that can be divided into three groups. Zircon dates of group-1 were analyzed on zircon cores with oscillatory zoning, suggesting their magmatic origin. They yield weighted mean  $^{207}\text{Pb}/^{206}\text{Pb}$  ages of 2.53–2.50 Ga, which is considered as the intrusion of granitoid gneisses. Zircon dates of group-2 were analyzed on zircon rims or grains with fir-leaf, sectorial or banded zoning, suggesting their metamorphic origin. Metamorphic zircons yield mean  $^{207}\text{Pb}/^{206}\text{Pb}$  ages of 2.51–2.49 Ga. They are interpreted as the timing of granulite facies metamorphism, which is coeval with the formation of pegmatite. Much attention should be paid to distinguish the magmatic and metamorphic zircons, especially when they exhibit no diagnostic feature in the CL image, because of their overlapped ages of ~2.50 Ga. Generally, the characteristics of Th/U ratios, CL images and REE patterns were proved to be effective method to address this issue. However, high Th/U ratios may also be common feature of zircons formed during high-grade metamorphic conditions [61]. Magmatic zircons from the concerned samples in this study have oscillatory zoning or structureless dark domains in the cores and are enriched in HREE, compared with metamorphic zircons that show fir-leaf, sectorial or banded zoning and low HREE contents (Figures 5 and 7). Group-3 zircon grains were analyzed on zircon cores with banded or structureless dark domains and yielded younger  $^{207}\text{Pb}/^{206}\text{Pb}$  ages of 2.45–2.01 Ga. Most of them were discordant, having suffered ancient loss of radiogenic Pb. We preferred to regard this younger age group as of no geological significance even though there are a few concordant ages of 2.4–2.3 Ga, because the U–Pb system of zircons may be partially reset by granulite facies metamorphism in a dry rock system, and the ages between the oldest and youngest are chronologically meaningless.

Besides, only one analysis performed on metamorphic zircon grain (spot #28) from sample J1349 in Saheqiao yielded the youngest and concordant  $^{207}\text{Pb}/^{206}\text{Pb}$  ages of  $1912 \pm 9$  Ma, indicating a Paleoproterozoic metamorphic event. In fact, abundant metamorphic zircon ages of 1.88–1.78 Ga have been identified from the metabasic dykes in the Qianxi and Qian'an area, and according to Duan et al. (2015, 2019) [32,33], the metabasic dykes, whose protolith age was ~2.1 Ga, have suffered HP granulite facies metamorphism at 1.84–1.82 Ga, with clockwise P–T path correlated to a crustal thickening event. However, the Paleoproterozoic zircon ages of ~1.80 Ga were quite difficult to be obtained from the ~2.5 Ga TTG and supracrustal rocks which should also have been subjected to HP granulite facies metamorphism in Paleoproterozoic. Yang et al. (2017) [36] obtained some metamorphic age data of ~1.80 Ga from Neoproterozoic mafic granulite by using zircon U–Pb isotopic methods. The reasonable explanations why metamorphic age of ~1.80 Ga was rarely obtained from Archean rocks might be as follows. (i) The Archean rocks have suffered granulite facies or UHT metamorphism, accompanied with melt loss and forming a dry rock system. Therefore, there would be very few melt and zircon generated during the Paleoproterozoic overprinting metamorphism of HP granulite facies, unless outside fluid or melt was injected into the dried rocks; (ii) metamorphic ages of 1.80 Ga were empirically obtained from zircon grains with small size (<50  $\mu\text{m}$ ) which show fir-leaf or sectorial zoning, or from the outermost metamorphic growth rim (<35  $\mu\text{m}$ , 5–25  $\mu\text{m}$  common) with relative high luminescence. And as such, there are only very few ~1.80 Ga zircon data being obtained from Neoproterozoic TTG gneisses and supracrustal rocks in Eastern Hebei although a lot of zircon U–Pb geochronological results have been reported in the published literature before [62]. In addition, the Lu–Hf garnet-whole rock isochron method was applied to garnet-bearing mafic granulites from the Saheqiao belt and yielded ages of 1787–1766 Ma, providing an alternative way to identify the Paleoproterozoic metamorphism from the Neoproterozoic rocks in Eastern Hebei [36].

### 5.1.2. Two Phases of Granulite Facies Metamorphism

The Neoproterozoic granulite facies metamorphism was considered to have anticlockwise P–T path involving an IBC process with the peak temperature condition of 780–940 °C

using conventional Fe–Mg exchange thermometers and phase equilibria modeling [31,48]. However, these temperature conditions of granulites are commonly underestimated because of the fast Fe–Mg diffusion during cooling process [63–66]. Recent studies suggest that the peak temperature of supracrustal rocks (mafic and pelitic granulites) in the Saheqiao linear-structural belt and Taipingzhai ovate-structural domain reaches UHT (>900 °C) conditions. Evidence supporting this are (1) petrographic observations reveal that the hornblende was formed later than the peak minerals of clinopyroxene and orthopyroxene in the mafic granulite (Figure 3e). Dehydration melting experiments of meta-basalts with tholeiitic to quartz tholeiitic compositions show that amphibole-out occurs chiefly at 1000–1100 °C [67–69]. Moreover, phase modeling for a MORB composition suggest that the stability limits of amphibole (am-out) are beyond 970 °C under 10 kbar, similar to the experimental results; (2) the calculated P–T pseudosections for pelitic granulites show that the observed peak assemblage, characteristic of the absence of the matrix biotite (Figure 3g,h), record temperature condition of >950 °C [34]; (3) P–T estimation using major element- and REE-based thermobarometers yield UHT conditions of 950–1100 °C for the clinopyroxene-orthopyroxene pair in mafic granulites from the Taipingzhai, Saheqiao and Qian’an area [35]. The paleoproterozoic metamorphism is considered to be of high pressure granulite facies with clockwise P–T path [32]. The overprinting mineral assemblages of paleoproterozoic metamorphic episode are well preserved in the mafic dyke samples. The diagnostic overprinting mineral assemblages in the orthogneisses and felsic paragneisses are identified by typical ‘red-eye socket’ texture (e.g., Figure 3e,f), with garnet-quartz coronas ( $g_2$ ) around peak two-pyroxene dominated assemblage. These coronary garnet grains were selected from mafic granulites for garnet-whole rock Lu–Hf isotopic analysis, yielding well-defined garnet-whole rock isochron ages of ~1.78 Ga similar to the aforementioned Paleoproterozoic metamorphic zircon ages of ~1.8 Ga from metabasic dykes and their surrounding rocks. The Paleoproterozoic overprinting mineral assemblage characterized by garnet coronas ( $g_2$ ) from pelitic granulites defined the same P–T condition as those recovered from Paleoproterozoic metabasic dykes [16–18], further proving that the garnet coronas ( $g_2$ ) were formed by Paleoproterozoic overprinting metamorphism of HP granulite facies [33].

### 5.2. Implications for the Tectonic Evolution

The tectonic setting of the Eastern Hebei during the late Neoproterozoic era has long been an issue of major dispute. Horizontal tectonism has been proposed, which was supported by continental magmatic arc models related to subduction-collision [28–30]. Another prevalent view was vertical tectonism, supported by mantle plume model [24,62] and sagduction model [16,34,37]. Our new data, combined with previous results, support the sagduction model of vertical tectonism in the Eastern Hebei terrane during Neoproterozoic. Firstly, the Neoproterozoic dome-and-keel structures were preserved in Taipingzhai and Anziling area [16,21,31], which was totally at variance with the linear tectonic zone generated by subduction-collision. According to Zhao et al. (2021) [16], the granitic dome formed through a vertically upward movement, and the supracrustal rocks sank downwards to form the regional keel structure. The dome-and-keel structure formed at 2530–2500 Ma, which suggest that until the late Neoproterozoic era, the vertical tectonism was still a dominant tectonic regime in Eastern Hebei. Secondly, voluminous high-grade TTG gneisses were contemporaneously generated during the late Neoproterozoic era [25–30]. In this contribution, the granitoid gneisses were emplaced between  $2524 \pm 7$  and  $2503 \pm 12$  Ma, being subjected to granulite facies metamorphism during  $2508 \pm 10$  to  $2468 \pm 33$  Ma. The protoliths of the pelitic granulites were also deposited in the Late Neoproterozoic era, followed by high-grade metamorphism from  $2494 \pm 7$  to  $2485 \pm 10$  Ma. The contemporaneous magmatism, sedimentation and metamorphism in a very short time period suggest that tectonic regime in Eastern Hebei should be dominated by vertical tectonism. Thirdly, the Neoproterozoic tectonothermal events were considered to have been generated under a typical Archean hot orogenic belt [44], and the Shangying-Saheqiao-Malanyu linear-structural belt

(ITD) in Zunhua and Santunying-Taipingzhai granulite facies zones (IBC) in Qian'xi was considered as typical paired metamorphic belts. However, the Saheqiao linear-structural belt was considered to be a reworked domain during the Paleoproterozoic orogeny, rather than a Neoproterozoic high-grade metamorphic belt [36]. High grade metamorphism with anticlockwise P-T path was recognized from mafic and pelitic granulites [31,34–37], which was related to mantle plume activity [24] or Archean unique vertical tectonics in Eastern Hebei [40]. The sagduction process was interpreted as mechanically short-lived, involving rapid burial and exhumation of supracrustal rocks, coeval with the peak of magmatic activity in contrast to subduction [37].

## 6. Conclusions

Based on geological observations, geochemical and geochronological data, and metamorphic evolution of the granitoid gneisses and supracrustal rocks in the Eastern Hebei terrane, major conclusions are drawn as follows:

1. The granitoid gneisses with dominant TTG compositions were emplaced from  $2524 \pm 7$  to  $2503 \pm 12$  Ma, and they have been subjected to Neoproterozoic granulite facies metamorphism during  $2508 \pm 10$  to  $2468 \pm 33$  Ma, coeval with the intrusion of pegmatite ( $2488 \pm 5$  Ma). The protoliths of the pelitic granulites were deposited in the Late Neoproterozoic era, followed by high-grade metamorphism from  $2494 \pm 7$  to  $2485 \pm 10$  Ma.
2. Zircon ages of 2.45–2.01 Ga in TTG gneisses and supracrustal rocks are considered to be of no geological significance. The Paleoproterozoic zircon ages (1.9–1.8 Ga), indicating an overprinting metamorphic event, are usually neglected. Empirically, the zircon grains of 1.9–1.8 Ga were extremely small or too narrow to be recognized and/or analyzed in the Archean TTG gneisses and supracrustal rocks.
3. Vertical tectonism was dominant in the Eastern Hebei terrane during the late Neoproterozoic era.

**Supplementary Materials:** The following supporting information can be downloaded at: <https://www.mdpi.com/article/10.3390/min12070863/s1>, Table S1: LA-ICP-MS U-Pb data of zircons; Table S2: REE data of Zircons.

**Author Contributions:** C.W. and Z.D. conducted the field observations and sampling. C.W. and C.Z. conceived and designed the experiments. Z.D. and Z.L. performed microscopic observations in petrographic microscope and the experiments of whole-rock geochemical compositions and zircon U-Th-Pb isotopic data. All the authors discussed the analytical results and prepared the manuscript and figures. All authors have read and agreed to the published version of the manuscript.

**Funding:** This work was financially supported by the National Natural Science Foundation of China (Grant Nos. 41902060) and the Natural Science Foundation of Hebei Province of China (Grant Nos. D2021403037).

**Data Availability Statement:** Not applicable.

**Acknowledgments:** We appreciate anonymous reviewers for their thoughtful and constructive reviews on the manuscript. We thank Ting Liu and Jie Dong for their help in experimental analyses. Jiahui Qian, Shiwei Zhang and Chuan Yang are gratefully acknowledged for their help in the field work.

**Conflicts of Interest:** The authors declare no conflict of interest.

## References

1. Condie, K.C. Archean greenstone belts. *Earth-Sci. Rev.* **1981**, *18*, 95–96.
2. Stephen, M.; Fernando, A.; Hanna, J.E. Proterozoic crustal extension and the generation of dome-and-keel structure in an Archean granite–greenstone terrane. *Nature* **1992**, *357*, 491–493.
3. Moyen, J.F.; Stevens, G. Experimental constraints on TTG petrogenesis: Implications for Archean geodynamics. *Am. Geophys. Union* **2006**, *164*, 149–175.

4. Timothy, M.K.; Brian, F.W.; Ali, P. Geological evidence for the operation of plate tectonics throughout the Archean: Records from Archean Plaeo-plate boundaries. *J. Earth Sci.* **2018**, *29*, 1291–1303.
5. Collins, W.J.; Van Kranendonk, M.J.; Teyssier, C. Partial convective overturn of Archaean crust in the East Pilbara Craton, Western Australia; driving mechanisms and tectonic implications. *J. Structural. Geol.* **1998**, *20*, 1405–1424. [[CrossRef](#)]
6. Lin, S.F.; Beakhouse, G.P. Synchronous vertical and horizontal tectonism at latestages of Archean cratonization and genesis of Hemlo gold deposit, Superiorcraton, Ontario, Canada. *Geology* **2013**, *41*, 359–362. [[CrossRef](#)]
7. Zhao, G.C.; Zhai, M.G. Lithotectonic elements of Precambrian basement in the North China Craton: Review and tectonic implications. *Gondwana Res.* **2013**, *23*, 1207–1240. [[CrossRef](#)]
8. Brown, M. Duality of thermal regimes is the distinctive characteristic of plate tectonics since the neoproterozoic. *Geology* **2006**, *11*, 961–964. [[CrossRef](#)]
9. Brown, M.; Johnson, T. Metamorphism and the evolution of subduction on Earth. *Am. Mineral.* **2019**, *104*, 1065–1082. [[CrossRef](#)]
10. Stern, R.J. When and how did Plate Tectonics Begin? Theoretical and Empirical Considerations. *Chin. Sci. Bull.* **2007**, *52*, 578–591. [[CrossRef](#)]
11. Timothy, M.K. Plate tectonics in relation to mantle temperatures and metamorphic properties. *Sci. China Earth Sci.* **2020**, *63*, 634–642.
12. Zheng, Y.F.; Zhao, G.C. Two styles of plate tectonics in Earth's history. *Sci. Bull.* **2020**, *65*, 329–334. [[CrossRef](#)]
13. Lin, S.F.; Parks, J.; Heaman, L.M.; Simonetti, A.; Corkery, M.T. Diapirism and sagduction as a mechanism for deposition and burial of "Timiskaming-type" sedimentary sequences, Superior Province: Evidence from detrital zircon geochronology and implications for the Bordden Lake conglomerate in the exposed middle to lower crust in the Kapuskasing uplift. *Precambrian Res.* **2013**, *238*, 148–157.
14. Van Kranendonk, M.J.; Collins, W.J.; Hickman, A.H.; Pawley, M.J. Critical tests of vertical vs. horizontal tectonic models for the Archean East Pilbara Granite–Greenstone Terrane, Pilbara Craton, Western Australia. *Precambrian Res.* **2004**, *131*, 173–211.
15. Van Kranendonk, M.J.; Smithies, R.H.; Hickman, A.H.; Champion, D.C. Review: Secular tectonic evolution of Archean continental crust: Interplay between horizontal and vertical processes in the formation of the Pilbara Craton, Australia. *Terra Nova* **2007**, *19*, 1–38. [[CrossRef](#)]
16. Zhao, C.; Zhang, J.; Zhao, G.C.; Yin, C.Q.; Chen, G.K.; Liu, J.; Liu, X.G.; Chen, W.L. Kinematics and structural evolution of the Anziling dome and keel architecture in east China: Evidence of Neoproterozoic vertical tectonism in the North China Craton. *GSA Bull.* **2021**, *134*, 2115–2129. [[CrossRef](#)]
17. Liu, D.Y.; Nutman, A.P.; Compston, W.; Wu, J.S.; Shen, Q.H. Remnants of  $\geq 3800$  Ma crust in the Chinese part of the Sino–Korean craton. *Geology* **1992**, *20*, 339–342. [[CrossRef](#)]
18. Song, B.; Nutman, A.P.; Liu, D.Y.; Wu, J.S. 3800–2500 Ma crustal evolution in the Anshan area of Liaoning Province, northeastern China. *Precambrian Res.* **1996**, *78*, 79–94. [[CrossRef](#)]
19. Wilde, S.A.; Valley, J.W.; Kita, N.T.; Cavosie, A.J.; Liu, D.Y. SHRIMP U–Pb and CAMECA 1280 oxygen isotope results from ancient detrital zircons in the Caozhuang quartzite, Eastern Hebei, North China Craton: Evidence for crustal reworking 3.8 Ga ago. *Am. J. Sci.* **2008**, *308*, 185–199. [[CrossRef](#)]
20. Wu, F.Y.; Yang, J.H.; Liu, X.M.; Li, T.S.; Xie, L.W.; Yang, Y.H. Hf isotopes of the 3.8 Ga zircons in eastern Hebei Province, China: Implications for early crustal evolution of the North China Craton. *Chin. Sci. Bull.* **2005**, *50*, 2473–2480. [[CrossRef](#)]
21. Zhao, G.C.; Sun, M.; Wilde, S.A.; Li, S.Z. Late Archean to Paleoproterozoic evolution of the North China Craton: Key issues revisited. *Precambrian Res.* **2005**, *136*, 177–202. [[CrossRef](#)]
22. Zhao, G.C.; Wilde, S.A.; Cawood, P.A.; Sun, M. Archean blocks and their boundaries in the North China Craton: Lithological, geochemical, structural and P–T path constraints and tectonic evolution. *Precambrian Res.* **2001**, *107*, 45–73. [[CrossRef](#)]
23. Zhao, G.C.; Cawood, P.A.; Li, S.Z.; Wilde, S.A.; Sun, M.; Zhang, J.; He, Y.H.; Yin, C.Q. Amalgamation of the North China Craton: Key issues and discussion. *Precambrian Res.* **2012**, *222*, 55–76. [[CrossRef](#)]
24. Zhao, G.C.; Cawood, P.A. Precambrian Geology of China. *Precambrian Res.* **2012**, *222–223*, 13–54. [[CrossRef](#)]
25. Geng, Y.S.; Liu, F.L.; Yang, C.H. Magmatic event at the end of the Archean in Eastern Hebei Province and its geological implication. *Acta Geol. Sin.* **2006**, *80*, 819–833.
26. Yang, J.H.; Wu, F.Y.; Wilde, S.A.; Zhao, G.C. Petrogenesis and geodynamics of Late Archean magmatism in eastern Hebei, eastern North China Craton: geochronological, geochemical and Nd–Hf isotopic evidence. *Precambrian Res.* **2008**, *167*, 125–149. [[CrossRef](#)]
27. Nutman, A.P.; Maciejowski, R.; Wan, Y.S. Protoliths of enigmatic Archaean gneisses established from zircon inclusion studies: Case study of the Caozhuang quartzite, E., Hebei, China. *Geosci. Front.* **2014**, *5*, 445–455. [[CrossRef](#)]
28. Nutman, A.P.; Wan, Y.S.; Du, L.L.; Friend, C.R.L.; Dong, C.Y.; Xie, H.Q.; Wang, W.; Sun, H.Y.; Liu, D.Y. Multistage late Neoproterozoic crustal evolution of the North China Craton, Eastern Hebei. *Precambrian Res.* **2011**, *189*, 43–65. [[CrossRef](#)]
29. Guo, R.R.; Liu, S.W.; Santosh, M.; Li, Q.G.; Bai, X.; Wang, W. Geochemistry, zircon U–Pb geochronology and Lu–Hf isotopes of metavolcanics from eastern Hebei reveal Neoproterozoic subduction tectonics in the North China Craton. *Gondwana Res.* **2013**, *24*, 664–686. [[CrossRef](#)]
30. Bai, X.; Liu, S.W.; Guo, R.R.; Zhang, L.F.; Wang, W. Zircon U–Pb–Hf isotopes and geochemistry of Neoproterozoic dioritic–trondhjemitic gneisses, Eastern Hebei, North China Craton: Constraints on Petrogenesis and tectonic implications. *Precambrian Res.* **2014**, *251*, 1–20. [[CrossRef](#)]

31. Kwan, L.C.J.; Zhao, G.C.; Yin, C.Q.; Geng, H.Y. Metamorphic P–T path of mafic granulites from Eastern Hebei: Implications for the Neoproterozoic tectonics of the Eastern Block, North China Craton. *Gondwana Res.* **2016**, *37*, 20–38. [[CrossRef](#)]
32. Duan, Z.Z.; Wei, C.J.; Qian, J.H. Metamorphic P–T paths and Zircon U–Pb age data for the Paleoproterozoic metabasic dykes of high-pressure granulite facies from Eastern Hebei, North China Craton. *Precambrian Res.* **2015**, *271*, 295–310. [[CrossRef](#)]
33. Duan, Z.Z.; Wei, C.J.; Li, Z. Metamorphic P–T paths and zircon u–pb ages of Paleoproterozoic metabasic dykes in eastern Hebei and northern Liaoning: Implications for the tectonic evolution of the North China Craton. *Precambrian Res.* **2019**, *326*, 124–141. [[CrossRef](#)]
34. Duan, Z.Z.; Wei, C.J.; Rehman, H.U. Metamorphic evolution and zircon ages of pelitic granulites in eastern Hebei, North China Craton: Insights into the regional Archean P–T–t history. *Precambrian Res.* **2017**, *292*, 240–257. [[CrossRef](#)]
35. Yang, C.; Wei, C.J. Ultrahigh temperature (UHT) mafic granulites in the East Hebei, North China Craton: Constraints from a comparison between temperatures derived from REE-based thermometers and major element-based thermometers. *Gondwana Res.* **2017**, *46*, 156–169. [[CrossRef](#)]
36. Yang, C.; Wei, C.J. Two phases of granulite facies metamorphism during Neoproterozoic and Paleoproterozoic in the East Hebei, North China Craton: Records from mafic granulites. *Precambrian Res.* **2017**, *301*, 46–64. [[CrossRef](#)]
37. Liu, T.; Wei, C.J. Metamorphic evolution of Archean ultrahigh-temperature mafic granulites from the western margin of Qian’an gneiss dome, eastern Hebei Province, North China Craton: Insights into the Archean tectonic regime. *Precambrian Res.* **2019**, *318*, 170–187. [[CrossRef](#)]
38. Zhao, G.C.; Wilde, S.A.; Cawood, P.A.; Lu, L.Z. Thermal evolution of Archean basement rocks from the eastern part of the North China Craton and its bearing on tectonic setting. *Inter. Geol. Rev.* **1998**, *40*, 706–721. [[CrossRef](#)]
39. Lu, J.S.; Zhai, M.G.; Lu, L.S.; Zhao, L. P–T–t evolution of Neoproterozoic to Paleoproterozoic pelitic granulites from the Jidong terrane, eastern North China Craton. *Precambrian Res.* **2017**, *290*, 1–15. [[CrossRef](#)]
40. Wei, C.J. Neoproterozoic granulite facies metamorphism and its tectonic implications from the East Hebei terrane. *Acta Petrol. Sin.* **2018**, *34*, 35–52.
41. Zhai, M.G.; Santosh, M. The early Precambrian odyssey of North China Craton. A synoptic overview. *Gondwana Res.* **2011**, *20*, 6–25. [[CrossRef](#)]
42. Kusky, T.M. Geophysical and geological tests of tectonic models of the North China Craton. *Gondwana Res.* **2011**, *20*, 26–35. [[CrossRef](#)]
43. Kusky, T.; Li, J.; Santosh, M. The Paleoproterozoic North Hebei Orogen: North China craton’s collisional suture with the Columbia supercontinent. *Gondwana Res.* **2007**, *12*, 4–28. [[CrossRef](#)]
44. Liu, S.W.; Wang, W.; Bai, X.; Guo, R.R.; Fu, J.H.; Guo, B.R.; Hu, F.Y.; Wang, M.J. Lithological assemblages of Archean meta-igneous rocks in Eastern Hebei–Western Liaoning Provinces of North China Craton, and their geodynamic implications. *Earth Sci.* **2018**, *43*, 44–56. [[CrossRef](#)]
45. Bai, X.; Liu, S.; Guo, R.; Wang, W. A Neoproterozoic arc–back–arc system in Eastern Hebei, North China Craton: Constraints from zircon U–Pb–Hf isotopes and geochemistry of dioritic–tonalitic–trondhjemitic–granodioritic (DTTG) gneisses and felsic paragneisses. *Precambrian Res.* **2016**, *273*, 90–111. [[CrossRef](#)]
46. Liou, P.; Guo, J.H.; Huang, G.Y.; Fan, W.B. 2.9 Ga Magmatism in Eastern Hebei, North China Craton. *Precambrian Res.* **2019**, *326*, 6–23. [[CrossRef](#)]
47. Zhang, L.C.; Zhai, M.G.; Zhang, X.J.; Xiang, P.; Dai, Y.P.; Wang, C.L.; Pirajno, F. Formation age and tectonic setting of the Shirengou Neoproterozoic banded iron deposit in eastern Hebei Province: Constraints from geochemistry and SIMS zircon U–Pb dating. *Precambrian Res.* **2012**, *222–223*, 325–338. [[CrossRef](#)]
48. Sun, H.Y.; Xie, H.Q.; Liu, S.J.; Dong, C.Y.; Liu, D.Y.; Wan, Y.S. Archean magmatism and metamorphism in the Huangbaiyu–Yangyashan area, eastern Hebei Province: Evidence from SHRIMP zircon U–Pb dating. *Geol. Bull. China* **2016**, *35*, 27–42.
49. Sun, H.Y.; Dong, C.Y.; Xie, H.Q.; Wang, W.; Ma, M.Z.; Liu, D.Y.; Nutman, A.; Wan, Y.S. The formation age of the Neoproterozoic Zhuzhangzi and Dantazi Groups in Qinglong area, Eastern Hebei Province: Evidence from SHRIMP U–Pb zircon dating. *Geol. Rev.* **2010**, *56*, 888–898.
50. Lü, B.; Zhai, M.G.; Li, T.S.; Peng, P. Zircon U–Pb ages and geochemistry of the Qinglong volcano–sedimentary rock series in Eastern Hebei: Implication for 2500 Ma intra–continental rifting in the North China. *Precambrian Res.* **2012**, *208–211*, 145–160.
51. Wiedenbeck, M.; Hanchar, J.M.; Peck, W.H.; Sylvester, P.; Valley, J.; Whitehouse, M.; Andreas Kronz, Y.M. Further characterization of the 91500 zircon crystal. *Geostand. Geoanalytical Res.* **2004**, *28*, 9–39. [[CrossRef](#)]
52. Andersen, T. Correction of common lead in U–Pb analyses that do not report <sup>204</sup>Pb. *Chem. Geol.* **2002**, *192*, 59–79. [[CrossRef](#)]
53. Van Achterbergh, E.; Ryan, C.G.; Jackson, S.E.; Griffin, W.L. Data reduction software for LA–ICP–MS. Laser–Ablation–ICPMS in the earth sciences—principles and applications. *Miner. Assoc. Can.* **2001**, *29*, 239–243.
54. Ludwig, K.R. ISOPLOT 3.0: A geochronological toolkit for Microsoft Excel. *Berkeley Geochronol. Cent. Spec. Publ.* **2003**, *4*, 74.
55. Middlemost, E.A.K. Naming materials in the magma/igneous rock system. *Earth Sci. Rev.* **1994**, *37*, 215–224. [[CrossRef](#)]
56. Barker, F. Trondhjemite: Definition, Environment and Hypotheses of Origin. In *Trondhjemites, Dacites and Related Rocks*; Elsevier: Amsterdam, The Netherlands, 1979; pp. 1–12.
57. Corfu, F.; Hanchar, J.M.; Hoskin, P.W.O.; Kinny, P. Atlas of zircon textures. *Rev. Miner. Geochem.* **2003**, *53*, 469–500. [[CrossRef](#)]

58. Grant, M.L.; Wilde, S.A.; Wu, F.; Yang, J. The application of zircon cathodoluminescence imaging, Th–U–Pb chemistry and U–Pb ages in interpreting discrete magmatic and high-grade metamorphic events in the North China Craton at the Archean/Proterozoic boundary. *Chem. Geol.* **2009**, *261*, 155–171. [[CrossRef](#)]
59. Rubatto, D. Zircon trace element geochemistry: Partitioning with garnet and the link between U–Pb ages and metamorphism. *Chem. Geol.* **2002**, *184*, 123–138. [[CrossRef](#)]
60. Sun, S.S.; McDonough, W.F. Chemical and isotopic systematics of oceanic basalts: Implications for mantle composition and processes. *Geol. Soc. London Sp. Publ.* **1989**, *42*, 313–345. [[CrossRef](#)]
61. Wan, Y.S.; Liu, D.Y.; Dong, C.Y.; Liu, S.J.; Wang, S.J.; Yang, E.X. U–Th–Pb behavior of zircons under high-grade metamorphic conditions: A case study of zircon dating of meta-diorite near Qixia, eastern Shandong. *Geosci. Front.* **2011**, *2*, 137–146. [[CrossRef](#)]
62. Li, Z.; Wei, C.J.; Zhang, S.W.; Yang, C.; Duan, Z.Z. Neoproterozoic granitoid gneiss in Eastern Hebei, North China Craton: Revisited. *Precambrian Res.* **2019**, *324*, 62–85. [[CrossRef](#)]
63. Powell, R.; Holland, T.J.B. On thermobarometry. *J. Metamorph. Geol.* **2008**, *26*, 155–179. [[CrossRef](#)]
64. Pattison, D.R.M.; Chacko, T.; Farquhar, J.; McFarlane, C.R.M. Temperatures of granulite facies metamorphism: Constraints from experimental phase equilibria and thermobarometry corrected for retrograde exchange. *J. Pet.* **2003**, *44*, 867–900. [[CrossRef](#)]
65. Liang, Y.; Sun, C.G.; Yao, L.J. A REE-in-two-pyroxene thermometer for mafic and ultramafic rocks. *Geochim. Cosmochim. Acta* **2013**, *102*, 246–260. [[CrossRef](#)]
66. Sun, C.G.; Liang, Y. A REE-in-garnet–clinopyroxene thermobarometer for eclogites, granulites and garnet peridotites. *Chem. Geol.* **2015**, *393–394*, 79–92. [[CrossRef](#)]
67. Rushmer, T. Partial melting of two amphibolites: Contrasting experimental results under fluid-absent conditions. *Contrib. Miner. Petrol.* **1991**, *107*, 41–59. [[CrossRef](#)]
68. Rapp, R.P.; Watson, E.B. Dehydration Melting of Metabasalt at 8–32 kbar: Implications for Continental Growth and Crust–Mantle Recycling. *J. Petrol.* **1995**, *36*, 891–931. [[CrossRef](#)]
69. Stevens, G.; Clemens, J.D.; Droop, G.T.R. Melt production during granulite facies anatexis: Experimental data from “primitive” metasedimentary protoliths. *Contrib. Mineral. Petrol.* **1997**, *128*, 352–370. [[CrossRef](#)]